JOURNAL OF AIRCRAFT
Vol. 45, No. 1, January–February 2008

Tail-Sitter Vertical Takeoff and Landing Unmanned Aerial Vehicle: Transitional Flight Analysis

Daisuke Kubo* and Shinji Suzuki†
University of Tokyo, Tokyo 113-8656, Japan

DOI: 10.2514/1.30122

A new design for a tail-sitter vertical takeoff and landing unmanned aerial vehicle was proposed. A nonlinear mathematical model of the vehicle dynamics was constructed by combining simple estimation methods. The flight characteristics were revealed through a trim analysis and an optimized transitional flight path analysis by using the mathematical model. The trim analysis revealed the existence of a flight path constraint to avoid stall; the vehicle could not descend in low-speed flight without high-lift devices such as flaps and slats. These devices improved the descent performance. In particular, slats provided a substantial improvement; they enabled a descent rate of 2 m/s. In the optimized transitional flight path analysis, a level outbound transition without high-lift devices was achieved although a trimmed level flight at low speed, as was shown in the trim analysis, was not possible; this was because the outbound transition was an accelerative flight. On the contrary, without high-lift devices, the vehicle could not avoid climbing to avoid stall during inbound transitions. The slats provided a satisfactory improvement during the transition and enabled a level inbound transition. These results showed the necessity of leading-edge slats for the proposed tail-sitter vertical takeoff and landing unmanned aerial vehicle.

I. Introduction

MINI-UNMANNED aerial vehicles (UAVs) are suitable for several civilian applications because they have advantages over large UAVs with regard to operational costs, human resources, and readiness. However, based on the mini-UAV development experiences of the authors [1], there is a need for more advanced takeoff and landing performance for operating mini-UAVs. In civil operations of mini-UAVs, the selection of areas for takeoff and landing is sometimes difficult because of the presence of buildings, trees, and hills that obstruct the takeoff or landing paths. It is not a minor difficulty; on the contrary, it is a serious constraint in certain missions. However, vertical takeoff-and-landing-capable vehicles can takeoff and land in relatively small areas even if the areas are surrounded by tall obstacles. In this paper, a new design of a tail-sitter vertical takeoff and landing (VTOL) mini-UAV is proposed and the feasibility is considered.

Some special design and operating methods have been developed for improving takeoff and landing performance. For example, the Raven UAV uses a deep-stall descent technique and the BirdEye-500 [2] uses parachutes and air cushions to improve the landing performance. Although the deep-stall technique can help vehicles land in small areas, the descent rate is not slow enough for some kinds of precision payloads. Parachutes are very useful for emergency recovery, but they cannot tolerate high-wind conditions. On the other hand, although VTOL aircraft have the disadvantage of extra-weight for an augmented propulsion system, they have operational advantages such as soft and accurate landings.

Historically, many types of manned VTOL aircraft have been researched and developed [3], and there are also many VTOL UAVs, for example, Eagle-Eye [4], SkyTote [5], and GoldenEye [6]. Eagle-Eye is a tilt-rotor UAV, which is very sophisticated but at the same time it is complicated and costly. SkyTote and GoldenEye are tail-sitter VTOLs. The tail-sitter design has the advantage of not requiring variable mechanisms like other VTOL configurations. SkyTote is equipped with coaxial counter-rotating rotors for the propulsion system; GoldenEye is equipped with ducted propellers for propulsion and uses an independently trimmed wing design for the main wings that are used during horizontal flight. However, these complicated designs are not suitable for mini-UAVs with strict weight constraints. On the other hand, there are many radio-control (RC) acrobatic planes that can hover without any special devices using only one fixed-pitch propeller and standard control surfaces immersed in the propeller slip stream. Although pilot skill is important for the aggressive maneuvering, the acrobatic flights suggest the potential for new designs for tail-sitter vehicles. T-wing [7], with a similar simple concept, has a canard configuration. In this paper, a new design for a tail-sitter mini-UAV with a conventional tail-wing configuration is proposed.

II. Conceptual Design

A. Design Features

The new design of a tail-sitter mini-UAV shown in Fig. 1 is considered in this study. This design has the following special features:

1) A twin counter-rotating propeller configuration is used, which is advantageous because the mechanism is much simpler than the other candidates, such as coaxial counter-rotating propellers/rotors. Another advantage is the wide angular range of the forward view from the payload sensors positioned in the main fuselage.

2) The ailerons, rudders, and elevators immersed in the propeller slip stream are sufficient to enable attitude control even in low-speed and hovering flights. No complicated control devices such as cyclic pitch control systems for rotors are required for attitude control in low-speed flight.

3) With the exception of the standard control surfaces, there are no variable mechanisms. The tilt mechanisms of tilt-rotors, tilt-wings, and tilt-ducts would make the systems considerably more complicated. These mechanisms are not suitable for mini-UAVs.

Although helicopters and tilt-rotors can descend safely via autorotation in case of a power failure, a tail-sitter vehicle in hovering mode cannot recover in such a case. However, it is not a serious problem because such mini-UAVs are attritable, and hovering flight is limited to short times for takeoff and landing.

B. Operation Scenario

The assumed operation scenario for the proposed tail-sitter mini-UAV is as follows. In the takeoff phase, the vehicle takes off using a

Received 30 January 2007; revision received 12 August 2007; accepted for publication 24 September 2007.

*Graduate Student, Department of Aeronautics and Astronautics. Student Member AIAA.

†Professor, Department of Aeronautics and Astronautics. AIAA Member.

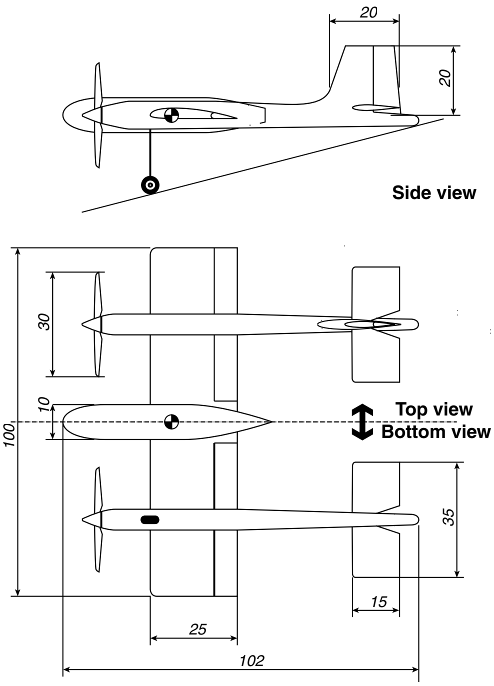

Fig. 1 Dimensions of the proposed tail-sitter mini-UAV (in centimeters).

support gear and climbs vertically to a certain altitude, which is determined from the location of the operation area. The vehicle then increases its flight speed and transitions to forward wing-borne flight; this is called an outbound transition. After the completion of the mission phase, the vehicle approaches the landing point. The vehicle gradually decreases its flight speed and transitions to hovering; this is called an inbound transition. During the final landing phase, the aircraft descends vertically and touches down with the tail gear; it then drops forward to touch down with the main gear.

III. Construction of Mathematical Model

A nonlinear simulation model was constructed to study the flight characteristics of the proposed tail-sitter mini-UAV. Considering the nature of this preliminary study, complex aerodynamic phenomena have not been discussed in detail. However, the stall characteristics and aerodynamic forces due to propeller slip streams must be evaluated because these are the most important characteristics of the tail-sitter.

A. Equations

To analyze a variety of flight conditions from zero-speed hovering motion to high-speed forward-flight motion, the following standard nonlinear equations of vehicle dynamics are considered.

$$\dot{U} = -QW - g\sin\theta + X_a/m \tag{1}$$

$$\dot{W} = QU + g\cos\theta + Z_a/(m + m_v) \tag{2}$$

$$\dot{\theta} = Q \tag{3}$$

$$J_Y\dot{Q} = M_a \tag{4}$$

$$\dot{X} = U\cos\theta + W\sin\theta \tag{5}$$

$$\dot{H} = U\sin\theta - W\cos\theta \tag{6}$$

Here, m and m_v denote the vehicle mass and virtual mass, respectively. The state variables such as U, W, and Q are defined in a general way [8]. The aerodynamic forces such as X_a, Z_a, and M_a in the equations are directly calculated using the estimation methods described in this section. The rotational dynamics of the motor and propeller are considered to be equivalent to the simple rotational motion of a first-order system, which is expressed as

$$J_{pm}\dot{\omega} = T_m - Q_p \tag{7}$$

Here, T_m is the motor torque, Q_p is the propeller drag torque, and J_{pm} is the total equivalent axial moment of inertia of the motor rotator, propeller, and spinner, which is identified by experiments as $J_{pm} = 5.7 \times 10^{-4}\ \mathrm{kg \cdot m^2}$.

B. Propeller Model

1) Calculation Method

The blade element/momentum theory and Glauert's hypothesis [9] were used for the propeller forces and the induced velocity estimations. A uniform distribution was assumed for the induced velocity, and the rotational component of the slip stream was ignored. The estimated values of the propeller thrust and torque were evaluated using experimental data. The variation in induced velocity with axial distance was considered to estimate the slip stream velocity developed on each wing. The propeller-induced velocity at a distance s from the propeller disk was assumed to be $v = k_s v_0$, where k_s is modeled using the equation described in [10]. Then, the diameter of the stream tube d_s at a distance s is also obtained [10].

2) Construction of Metamodel

Although the computational cost for the one-time calculation of the propeller model is not considerable, the total computational costs for the trim analysis and optimization analysis cannot be neglected; this is because the calculation code is run repeatedly during these processes. To reduce computations, a metamodel was constructed using a radial basis function network (RBFN) technique; the metamodel is a simplified model that approximates the relationship between the inputs and outputs of the original model. The MATLAB neural network toolbox was used for learning the Gaussian RBFN [11]. The learning procedure was based on the orthogonal least-squares method [11] and was provided in the toolbox. Three RBFNs were constructed for thrust T_p, propeller drag torque Q_p, and induced velocity v, respectively. The inputs for the networks are propeller rotation speed ω and airspeed U_p and W_p in the propeller axis. To choose better sampling points from the input space, the Latin hypercube sampling [12] was used.

C. Motor Model

Electric dc brushless motors are assumed for the propulsion. In the model aircraft market, the specifications of the motors are usually expressed using three parameters: the Kv constant, K_V, rpm/V; internal resistance R_m, Ω; and no-load current I_0, A. The motor torque can be approximately calculated from these parameters using the following equation.

$$T_m = K_t(V_e/R_m - I_0)\{1 - (K_t/V_e)\omega\} \tag{8}$$

Here, K_t, N m/A is the torque constant, and is related to the Kv constant as $K_t = (60/2\pi)/K_V$. The following values are assumed: $K_V = 985$ rpm/V, $R_m = 0.04\ \Omega$, and $I_0 = 2$ A. In this study, the input voltage V_e to the motor is assumed to be equal to the throttle setting δ_{thr}.

D. Aerodynamic Forces Acting on the Wings

The aerodynamic characteristics of the immersed wings are a dominant factor in the tail-sitter concept. Large parts of the wing surfaces are immersed in the propeller slip streams. The actual fluid-dynamic behavior around the propeller-wing combination is very complicated. Although computational fluid dynamics may have the potential to solve the problem, the procedure involves considerable computational costs when applied to conceptual design processes. The focus of this paper is not the accuracy of the aerodynamic prediction itself but the estimation of the qualitative flight characteristics. Therefore, simple methods are preferred.

Estimation Procedure

Step 1: The curves of the nondimensional wing aerodynamic coefficients C_L, C_D, and C_m against the angle of attack (AoA) α are estimated [13] for the main, horizontal, and vertical wings without considering the propeller slip-stream effect. Aerodynamic coefficients for an NACA0012 airfoil [14] and NACA4412 airfoil [15] are used as the base data for determining the aerodynamic characteristics of the airfoils. The former is used for the horizontal wing and vertical fin, and the latter is used for the main wing. Although the NACA0012 airfoil data [14] contains the aerodynamic coefficients at all angles of attack from −180 to +180 deg, the NACA4412 airfoil data [15] is confined to the range −16 to +20 deg. Modified NACA0012 data are used to interpolate for the range of the AoA for which NACA4412 data are not available.

Step 2: Each wing is divided into immersed and nonimmersed portions. The width of the immersed portion is estimated to be equal to the diameter of the propeller slip-stream tube d_s (Sec. III.B) at the 25% chord position for each wing.

Step 3: The aerodynamic forces acting on the nonimmersed portions of the main wing $[L, D, M]_{\text{nonimmersed}}$ are calculated by using the freestream airspeed V, total area S_{ni} of the nonimmersed portion of the wing, the freestream AoA α, and the wing aerodynamic coefficients constructed in step 1.

Step 4: The aerodynamic forces acting on the immersed portions of the main wing $[L, D, M]_{\text{immersed}}$ are calculated by using the propeller slip-stream speed V_s, the total area S_{im} of the immersed portion of the wing, slip-stream AoA α_s, and the wing aerodynamic coefficients. The AoA α_s is computed using the propeller slip-stream velocity, which is the resultant velocity of the external freestream velocity $\boldsymbol{V}$ and the propeller-induced stream velocity $k_s\boldsymbol{v}$.

Step 5: It is assumed that the imaginary induced downwash angles caused by airflow around the immersed portions and nonimmersed portions are estimated using following equations.

$$\varepsilon_{\text{im}} = C_L(\alpha_s)/\pi AR \quad \text{and} \quad \varepsilon_{\text{ni}} = C_L(\alpha)/\pi AR \tag{9}$$

Here, AR is an aspect ratio of the main wing. The actual downwash angle ε for the horizontal wing is estimated as a weighted average of ε_{im} and ε_{ni} using weighting factors $S_{\text{im}}q_{\text{im}}$ and $S_{\text{ni}}q_{\text{ni}}$, respectively. Here, q_{im} and q_{ni} represent the dynamic pressure on the immersed and nonimmersed portions of the main wing, respectively.

Step 6: The aerodynamic forces acting on the horizontal wings and vertical fins are calculated in a manner similar to steps 1–4. In particular, the downwash angle ε factors into the calculations pertaining to the horizontal wings. These forces are transformed to those acting on the center of gravity of the vehicle, considering moment arms.

E. Effects of High-Lift Devices

The trailing-edge flaps and leading-edge slats were also modeled using data described in [15] and methods described in [13]. For the plain flaps, 30% of the wing chord and a deflection angle δ_f of 20 deg were considered, whereas for the slats, an extended chord ratio c_s/c of 1.1 and δ_s of 20 deg were assumed. Although almost all these estimation methods were obtained for small angles of attack, they are used for all the values of the angle in this study. This assumption is reasonable because regions with large angles of attack are not dominant during flights without stall, which are the focus of this study.

F. Stall Angles of Attack

The following stall angles of attack $\alpha_{w,\text{stall}}$ are assumed for the main wing for the conditions listed in Table 1. These values are derived in the aerodynamic coefficient estimation process. It is assumed that the immersed portions of wings are relatively large compared with the nonimmersed portions. Therefore, the stall constraints of the immersed portions are crucial in this study.

Table 1 Stall angles-of-attack values settings

Configuration	$\alpha_{w,\text{stall},l}$, deg	$\alpha_{w,\text{stall},u}$, deg
With HLDs	−15	+15
With flaps	−20	+14
With slats	−15	+25
With flaps and slats	−20	+24

G. Other Components

The fuselage drag coefficient C_{Df} at $\alpha = -180, 0, +180$ deg and at $\alpha = -90, +90$ deg is assumed to be 0.1 and 1.0, respectively. These values are defined based on the frontal area of the fuselage. The C_{Df} curves for α values between the aforementioned values are obtained through interpolation by using the curve of the drag coefficient for the NACA0012 airfoil [15] for α values between 0 and +90 deg. The pitching moment is calculated using the slender body theory, which is expressed by the following equation.

$$M_{\text{fus}} = (1/2)\rho V^2 V_{\text{fus}} \sin(2\alpha) \tag{10}$$

The total drag force due to the other components such as a landing gear is assumed to be $C_{\text{Dg}} = 0.01$ based on main-wing area, and it is independent of α. This drag force is assumed to act toward the center of gravity of the vehicle.

H. Inertia Model

The total vehicle mass is assumed to be 2 kg. The aircraft is divided into components such as wings, fuselage, motors, batteries, and payload, which can be assumed to have basic shapes such as cubes, plates, or ellipsoids; moreover, it is assumed that each component is uniform in density. Under such an assumption, the moments of inertia are calculated for each component, and the total moment of inertia of the vehicle is estimated as $J_Y = 0.059\ \text{kg} \cdot \text{m}^2$.

IV. Trim Analysis

An analysis of the steady-state trimmed flight conditions existing between hovering and horizontal flight is important to obtain insight regarding transitional flights. To obtain trimmed flight conditions, the system of equations $\dot{U} = \dot{W} = \dot{Q} = \dot{\omega} = 0$ is solved numerically. Here, six variables, U, W, θ, ω, δ_{ele}, and δ_{thr}, are unknown. The flight path angle γ and the airspeed V are conditional parameters; the trimmed conditions over the flight envelope are obtained for these two parameter settings.

A. Results of Clean Configuration

The results are shown in Fig. 2. The radial axis indicates V, and the axial axis γ. The light continuous lines in the figures represent the contour lines of the trimmed pitch attitude. Three active constraint

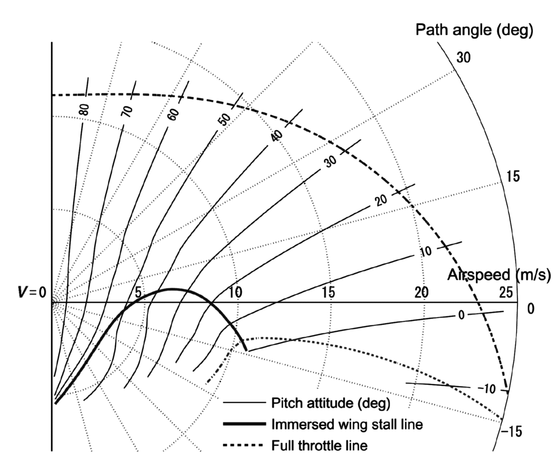

Fig. 2 Contour plot of the distribution of trimmed pitch attitude θ and constraints (without HLDs).

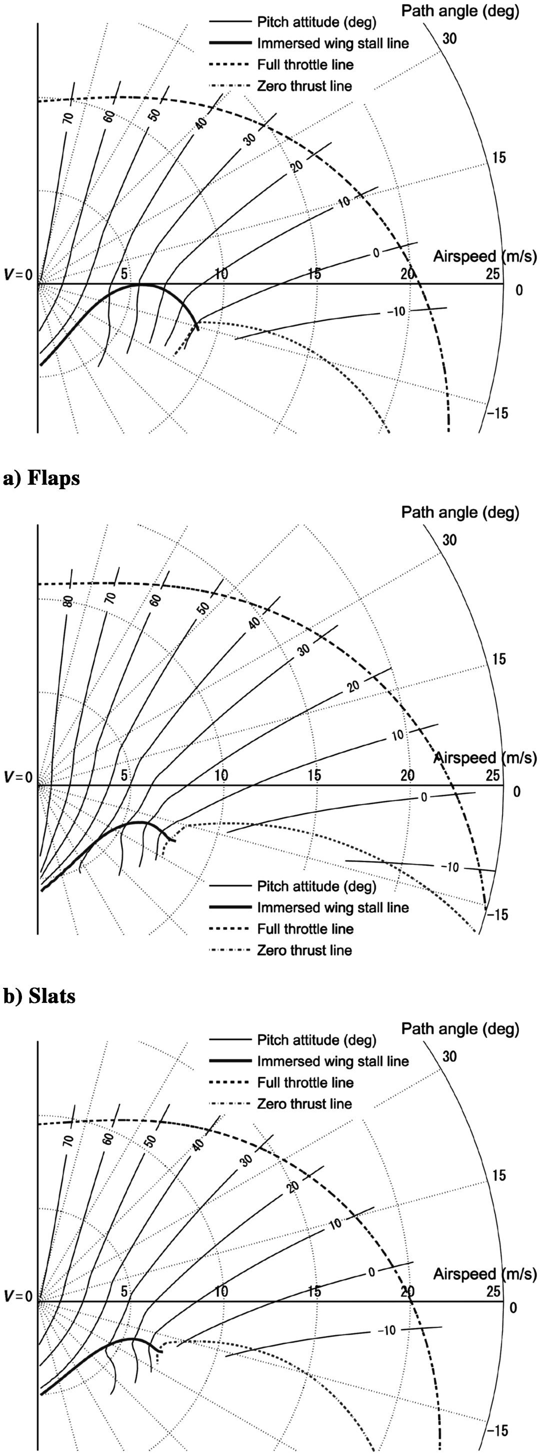

a) Flaps

b) Slats

c) Flaps + slats

Fig. 3 Contour plot of the distribution of trimmed pitch attitude θ and constraints (with HLDs).

lines are also shown in the plot. The dark broken line indicates trimmed flight with full throttle settings. The light broken line indicates a flight condition with zero propeller thrust. The dark continuous line indicates flight conditions at which the immersed portion of the main wing stalls. The vehicle can fly steadily only within the area enclosed by these constraint lines. A horizontal-tail stall constraint is not critical in trimming flights.

The results indicate that feasible trimmed flight conditions exist continuously from hover to horizontal flight. However, if V ranges from approximately 4 to 8 m/s, a positive value of γ is needed to avoid stalling the immersed wing. It is a serious problem because it implies that the vehicle cannot descend at certain airspeeds. Wind is present in actual flight conditions, and wind speeds greater than 4 m/s are not rare. Therefore, this constraint is unacceptable.

B. Effects of High-Lift Devices

Trimmed flight conditions were obtained for the following three high-lift device (HLD) settings: a) flaps, b) slats, and c) flaps + slats. The results are plotted in Fig. 3. In Fig. 3a, the constraint line for the stall shifts slightly toward the negative direction of γ because the flaps increase lift and cause the trimmed attitude θ and the AoA α to decrease. However, because the stall angle of the wing itself is slightly reduced from +15 to +14 deg, the improvement is not significant. In Fig. 3b, the constraint line shifts considerably toward the negative direction of γ because the slats directly relax the constraint relating to the stall angle of the wing. In Fig. 3c, although the trimmed θ decreases, the constraint line for the stall is almost similar to that obtained in Fig. 3b; there is very small improvement over Fig. 3b. In Figs. 3b and 3c, a descent rate over 2 m/s is possible over the entire airspeed region.

V. Optimized Transitional Flights Analysis

The characteristics of feasible transitional flights are analyzed by computing typical flight trajectories by using a trajectory optimization program equipped with sequential quadratic programming [16]. This approach provides only optimal feed-forward control input; it is an ideal solution. However, it provides some insights about the limitations of feasible transitional flights.

A. Constraints

The constraints represented in Table 2 are assumed to obtain reasonable transitional flight trajectories. See also Table 1 for the specific values of $\alpha_{w,\mathrm{stall},l}$ and $\alpha_{w,\mathrm{stall},u}$.

B. Objective Function

Typical optimal flight paths are calculated by minimizing the following objective function.

$$J = w_1 t_f + w_2 \int_0^{t_f} \Delta H^2 \,\mathrm{d}t + \int_0^{t_f} (w_3 \dot{\delta}_{\mathrm{ele}}^2 + w_4 \dot{\delta}_{\mathrm{thr}}^2)\,\mathrm{d}t \qquad (11)$$

The last two terms are used to avoid very rapid changes in the inputs. The values of w_i ($i = 1, 2, 3, 4$) are the weight factors.

C. Optimized Outbound Transitions

Figure 4 shows outbound transitions from zero-speed steady hovering to a steady level forward-flight with an airspeed of 16 m/s. The broken line denotes the flight trajectory. The arrows show the pitch attitude and the position of the vehicle. These arrows are plotted at intervals of $0.1 \times t_f$ s. The following values are used as the weight factors: $\boldsymbol{w}_1 = (1, 0, 10^{-3}, 10^{-7})$. The intent is to realize the "fastest transitions." The vehicle is able to transition from hover to forward-flight without altitude changes. Because the outbound transition is an accelerating flight, the throttle settings are high. The propeller slip streams then become stronger than those during the trimmed flight condition. Therefore, main-wing stall is delayed and a horizontal transition becomes possible despite the impossibility of a trimmed level flight without HLDs in some airspeed ranges (see Sec. IV). Considering the practical operation of the UAV, the vehicle does not

Table 2 Constraints of flight

Constrained parameters	Lower constraint	Upper constraint
Main-wing AoA, α_{ws}	$\alpha_{w,\mathrm{stall},l}$	$\alpha_{w,\mathrm{stall},u}$
Horizontal-wing AoA, α_{hs}	−15 deg	+15 deg
Rate of climb, $\dot{H}$	0 m/s	——
Pitch angle, θ	−10 deg	+100 deg
Throttle setting, δ_{thr}	4 V	9.5 V

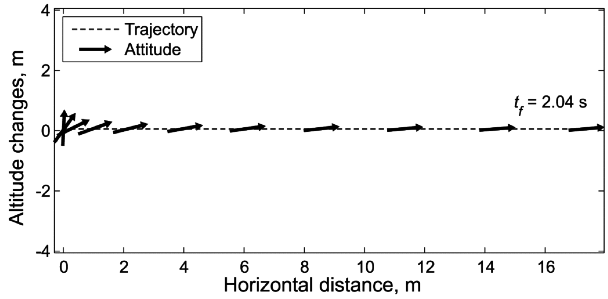

Fig. 4 Trajectory and attitude of the vehicle without HLDs for the fastest outbound transitional flight.

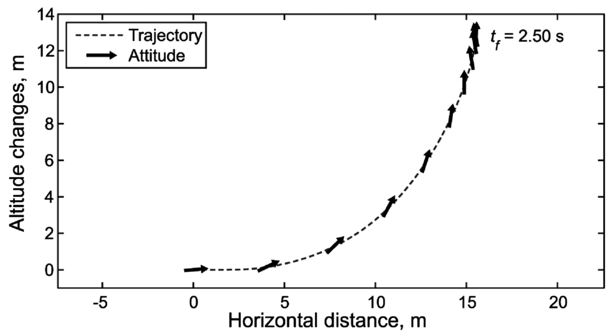

Fig. 5 Trajectory and attitude of the vehicle for the fastest inbound transitional flight without HLDs.

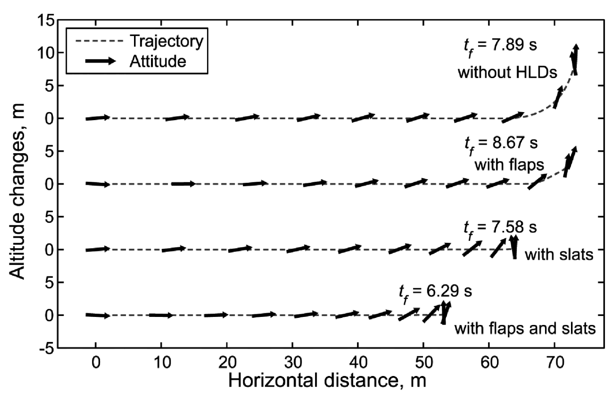

Fig. 6 Comparison of the optimal inbound transitional flights using weight factor w_2.

have to necessarily fly level during the outbound transition; climbing flight is more natural. An outbound transition with climbing fight is easier than a level transition because the throttle settings are higher, that is, the stall margin is increased. Therefore, this result shows that even difficult cases of outbound transitions are possible.

D. Optimized Inbound Transitions

As shown in Fig. 5, the fastest inbound transition from a steady level forward-flight to steady hover is during climbing flight. The values of $\boldsymbol{w}_1$ are also used to calculate this flight path. Pitching up and climbing are needed to rapidly reduce the speed. It is thought that climbing flight is required to avoid stall because decelerating flight cannot create a slip stream stronger than that during accelerating flight. However, this is not desirable, because climbing flight is not suitable for landing. In practice, smaller altitude changes are desirable.

To obtain flight trajectories with small altitude changes, the following weight factor is tested: $\boldsymbol{w}_2 = (0.1, 1, 0.1, 10^{-5})$, and the results are shown in Fig. 6. In the cases without HLDs and with flaps, the flight paths become flatter than that in Fig. 5, but the vehicle cannot avoid climbing. Although many other weight factor settings were tried, climbing in inbound transition is unavoidable in these cases. However, leading-edge slats improve the transitions. In the cases with slats and with flaps and slats, the vehicle can transition without climbing from forward-flight to hovering. Such completely flat transitions are not necessarily required in practical flight; however, the results show an increase in the maneuverability due to the use of leading-edge slats. Leading-edge slats are also important for dynamic transitional flight as well as steady trimmed flight.

VI. Conclusions and Future Work

A new design for a tail-sitter mini-UAV was proposed and its features and operational concepts were discussed. A mathematical model of the vehicle was constructed using simple estimation methods. Trim analysis using the mathematical model revealed the important characteristics for steady trimmed flight. Slats and flaps can improve descent performance. Slats are particularly important in improving the performance and in decreasing the minimum possible flight path angle; the vehicle can descend at a rate of 2 m/s at any airspeed. This is a very important characteristic because it implies that the vehicle can hover and vertically descend under any wind-speed conditions. The optimization process for the transitional flight trajectories revealed that a level outbound transition was possible without any HLDs; however, level inbound transition was not possible without HLDs. Slats make level inbound transition possible.

Although these analyses were based on simple models, a model plane based on our analysis will be constructed to verify our concept. The results showed the necessity of leading-edge slats for the tail-sitter mini-UAV; this information will be useful in designing practical vehicles and flight controllers. Practical controllers for transitional flight remain an area for future work.

Acknowledgment

The present research was supported in part through the Innovative Aerial Robot Project under the 21st Century Center of Excellence Program "Mechanical Systems Innovation" by the Ministry of Education, Culture, Sports, Science, and Technology.

References

[1] Kubo, D., Suzuki, S., and Kagami, T., "Development of Experimental Small UAV Equipped with Cellular Phone Data Link System," *Proceedings of 25th Congress of ICAS*, International Council of the Aeronautical Sciences ICAS-2006-1.7.3, 2006.

[2] Abershitz, A., Penn, D., Levy, A., Shapira, A., Shavit, Z., Tsach, S., "IAI's Micro/Mini UAV Systems-Development Approach," *Infotech@Aerospace*, AIAA Paper 2005-7034, 2005.

[3] Ranson, R., "An Overview of VSTOL Aircraft and Their Contributions," *AIAA International Powered Lift Conference and Exhibit*, AIAA Paper 2002-5979, 2002.

[4] Foster, M., "The Future Evolution of the Tiltrotor," *AIAA/ICAS International Air and Space Symposium and Exposition: The Next 100 Years*, AIAA Paper 2003-2652, 2003.

[5] Taylor, D. J., Ol, M., and Cord, T., "SkyTote: An Unmanned Precision Cargo Delivery System," *AIAA/ICAS International Air and Space Symposium and Exposition: The Next 100 Years*, AIAA Paper 2003-2753, 2003.

[6] Schaefer, C. G., Jr., and Baskett, L. J., "GoldenEye: The Clandestine UAV," *2nd AIAA "Unmanned Unlimited" Systems, Technologies, and Operations*, AIAA Paper 2003-6634, 2003.

[7] Stone, H., and Wong, K. C., "Preliminary Design of a Tandem-Wing Tail-Sitter UAV Using Multi-Disciplinary Design Optimization," *International Aerospace Congress*, The Royal Aeronautical Society, Australian Div., New South Wales, Australia, 1997, pp. 707–720.

[8] Stevens, B. L., and Lewis, F. L., *Aircraft Control and Simulation*, Wiley, New York, 1992.

[9] Gessow, A., and Myers, G. C., Jr., *Aerodynamics of the Helicopter*, Macmillan, New York, 1952.

[10] McCormick, B. W., Jr., *Aerodynamics of V/STOL Flight*, Academic Press, New York, 1967.

[11] Chen, S., Cowan, C. F. N., and Grant, P. M., "Orthogonal Least Squares Algorithm for Radial Basis Function Networks," *IEEE Transactions on Neural Networks*, Vol. 2, No. 2, 1991, pp. 302–309. doi:10.1109/72.80341

[12] Mckay, M. D., Beckman, R. J., and Conover, W. J. A., "Comparison of Three Methods for Selecting Values of Input Variables in the Analysis of Output of a Computer Code," *Technometrics*, Vol. 21, No. 2, 1979, pp. 239–245.
doi:10.2307/1268522

[13] Roskam, J., *Airplane Design Part 6: Preliminary Calculation of Aerodynamic*, Thrust and Power Characteristics, Roskam Aviation and Engineering, Ottawa, KS, 1990.

[14] Critzos, C. C., Heyson, H. H., and Boswinkle, R. W., Jr., "Aerodynamic Characteristics of NACA0012 Airfoil Section at Angles of Attack from 0 deg to 180 deg," NACA TN 3361, 1955.

[15] Abbott, I. H., and Von Doenhoff, A. E., *Theory of Wing Sections*, Dover, New York, 1959.

[16] Yokoyama, N., "A Study on Multidisciplinary Optimization and its Application to Conceptual Design of Space Plane," Ph.D. Dissertation, Aeronautics and Astronautics Dept., Univ. of Tokyo, 2005.